ACRS 2022
MONGOLIA

# EFFECTIVEB BAND OF SPOT-7 FOR LANDSLIDE DETECTION USING U-NET

Tomohisa Konishi [1], Seiji Ito [1] and Yoshinari Oguro [1]
[1]Hiroshima Institute of Technology, 2-1-1 Miyake, Saeki-ku, Hiroshima 731-5193, Japan,
Email: t.konishi.vd@cc.it-hiroshima.ac.jp; seiji@cc.it-hiroshima.ac.jp; y.oguro.yx@it-hiroshima.ac.jp

**KEY WORDS:** landslide monitoring; deep learning; machine learning; pan sharpening

**ABSTRACT:** Landslide disasters caused by heavy rains or earthquakes can have a serious impact on human lives and property. Earth observation satellite images are expected to be utilized to quickly identify disaster area. In recent years, deep learning-based segmentation has been gaining attention in the field of computer vision due to its improved performance. Therefore, we conducted to detect landslides using U-Net, a convolutional neural networks (CNN) that is considered effective in image recognition. The 2018 Hokkaido Eastern Iburi Earthquake was used as an example of a landslide detection. By the earthquake, many landslides occurred and claimed 36 lives. A binary landslide map as ground truth was used to train, validate, and test the model. Landslides were detected using SPOT-7 image observed on October 4, 2018. Pan-sharpened image was created using the High Pass Filter (HPF) resolution merge. We prepared four types of datasets including 4-band images for landslide detection, that is, (1) blue, green, red and NIR, (2) blue, green and red (3) green, red and NIR, (4) blue, green and NDVI. The U-Net learns from pairs of small patch images including the input and the ground truth images. From the dataset, 64% for training data, 16% for validation data, and 20% for test data. The U-Net was trained for 100 epochs with a mini-batch size of 8, 16, 24, 32, and 40. We used dice coefficient loss function and adaptive moment estimation (Adam) for the optimizer. The landslide detection results were validated by the F1-score. As the results, the highest value of the F1-score was obtained with the dataset (4). NDVI is more effective than original bands (red and NIR) for detecting landslide area. Our experiments in the test area showed that the deep learning model would provide rapid landslide detection for hazard assessment.

## 1. INTRODUCTION

Landslides are one of the most serious geological disasters that threaten human lives and property. This is because many people live on mountain slopes, which are prone to landslides, due to the mountainous terrain and narrow plains. Landslide detection and mapping are crucial for rapid disaster relief, recovery after the landslide, and assessment. Satellite imagery is considered the primary available data source for landslide detection. Landslides inventory maps are generally produced by visual interpretation of high-resolution satellite imageries (Zhong, 2020). Visual interpretation by an expert is highly accurate but time-consuming task, so it is not suitable for wide-area landslide detection and rapid response. Thus, an automated method of detecting landslides is needed. Landslide detection using satellite imagery has been performed by visual interpretation, image classification such as the maximum likelihood method, and artificial intelligence systems such as k-means, support vector machines. High spatial and temporal resolution of optical satellite observations enables more detailed and reliable identification of affected areas, an immediate response minimizing the risk of omission, and repeated observations potentially leading to multi-temporal inventories (Tofani, 2014). In recent years, machine learning approaches, including Convolutional Neural Networks (CNN), have been optimized to achieve results in remote sensing imageries. Machine learning is empirically learned using training data sets in feature extraction models. Fully Convolutional Networks (FCN) is a landmark in image segmentation (Long, 2015). FCN is a method using deep learning and consists of a convolutional layer and a pooling layer without using a fully connected layer. However, FCN generates a coarse segmentation map because of the loss of object location information during the pooling operation. U-Net (Ronneverger, 2015) uses deconvolution and skip connection to preserve the location information loss due to convolution process, enabling more precise image segmentation. The model originally applied to the segmentation of biomedical images. Some studies have applied U-net to landslide detection using satellite imagery. The U-Net model has been applied to landslide detection in the mountainous region of Rio de Janeiro, Brazil (Soares, 2020) and the Himalayan region of Nepal (Bragagnolo, 2021).

This research aims to evaluate how different band combination of optical satellite data impacts on the landslide detection accuracy of U-Net. We prepared four types of datasets including 4-band images for landslide detection, that is, (1) blue, green, red and near infrared (NIR), (2) blue, green and red (3) green, red and NIR, (4) blue, green and NDVI. U-Net model was trained and evaluated using landslide area in Hokkaido prefecture, Japan, induced by the 2018 Hokkaido Eastern Iburi Earthquake. The models derived from four datasets were evaluated in F1-score metric. The text is organized as follows: Section 2 presents the materials and methods, Section 3 presents the results and discusses the main implications of the findings, and Section 4 presents brief conclusion of this research.

## 2. MATERIALS AND METHODS

### 2.1 Study Site

The 2018 Hokkaido Eastern Iburi earthquake with an Mj (Japan Meteorological Agency (JMA) magnitude) 6.7 occurred at 03:07 am (local time) on 6 September, 2018 (JMA, 2018). There were 31 severe injuries and 42 deaths. 462 houses were completely destroyed by the earthquake. 1,570 houses were partly destroyed, and 12,600 houses were damaged (FDMA, 2019). There were a lot of landslides in Hokkaido prefecture triggered by the earthquake. The study area was the area of Abira and Mukawa Towns, centered on Atsuma Town, Hokkaido, as shown in the red rectangle in Figure 1. Many landslides occurred in this area due to the earthquake.

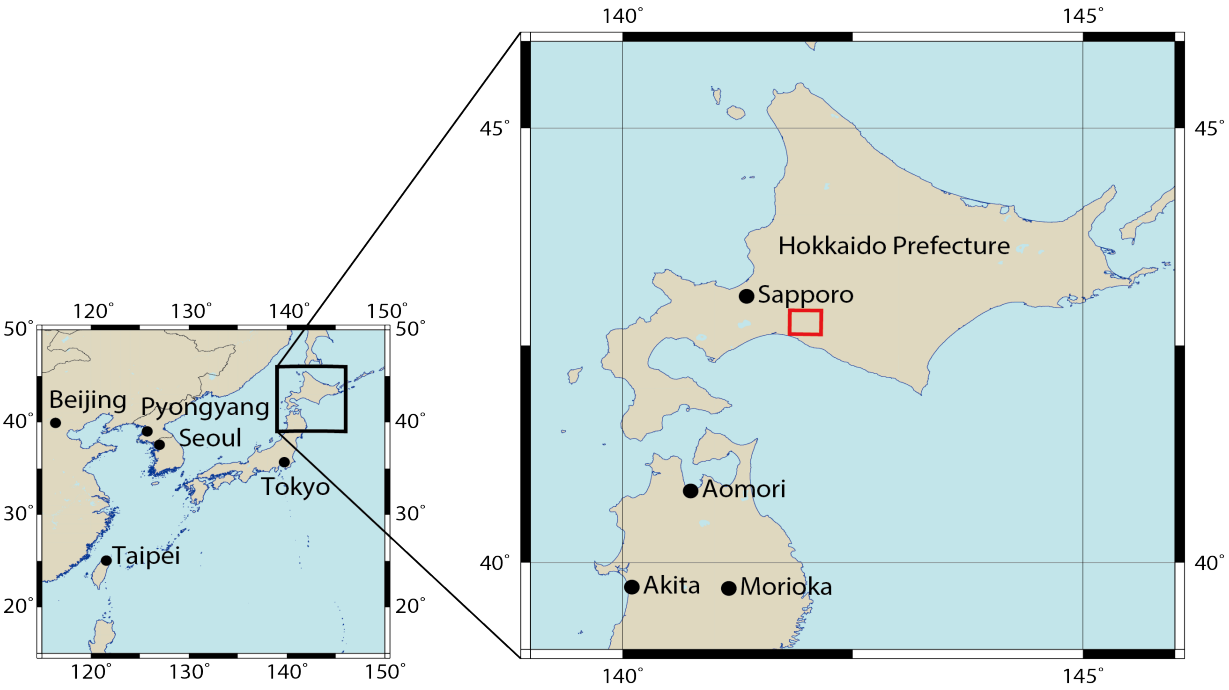


Figure 1. Map of study site in Japan (Red rectangle is study site).

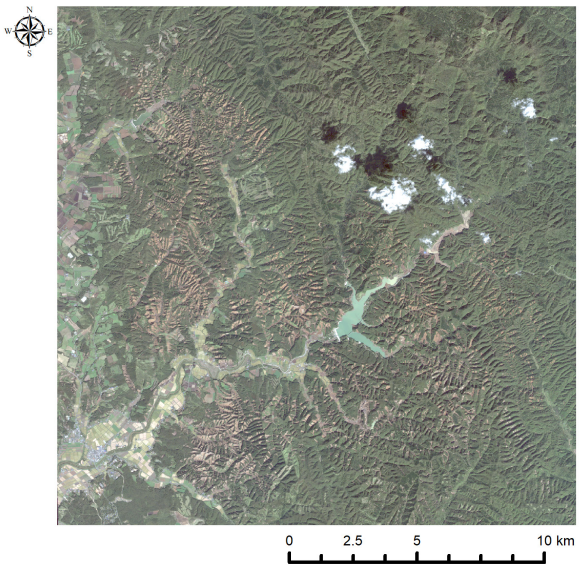


Figure 2. Pansharpened image of SPOT-7 in the test site (R: red, G: green, B: blue).

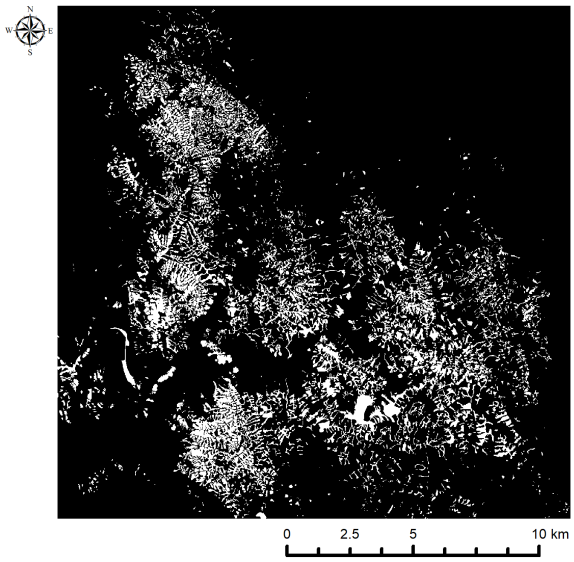


Figure 3. Validation image of landslide in the study site.

### 2.2 Data and Samples

SPOT-7 image acquired after the earthquake was used. New Astrosat Optical Modular Instrument (NAOMI) provides high-resolution panchromatic and multispectral (blue, green, red, and NIR) imageries. The panchromatic resolution is 1.5 m and the multispectral resolution is 6 m with 60 km swath. SPOT-7 image was acquired on 4 October 2018. SPOT-7 image was used Level3 (ortho) product with WGS 84/UTM 54N (EPSG: 32654) coordinate reference system. The study site is 25.6 km in width and 25.6 km in height. The pan-sharpened image was created with the High Pass Filter (HPF) resolution merge using the ERDAS IMAGINE. The HPF resolution merge combines high-resolution panchromatic data with lower resolution multispectral image, resulting in excellent detail and a realistic representation of original multispectral scene colors (Hexagon, 2022). The processed image was resolution of 1.5 m with 4 multi-spectral bands. Figure 2 shows the pan-sharpened image of SPOT-7 in the test site.

The geospatial information authority of Japan (GSI) took aerial photographs (ortho-photographs) of this area from September 5 to 11 in 2018, immediately after the earthquake. The GSI provides slope failure and sediment distribution map created by visual interpretation of those aerial photographs in GeoJSON format (GSI, 2018). A raster landslide map for validation was created from the vector data. Figure 3 shows the validation image of the landslide in the study site. The white color depicts the landslide area.

### 2.3 Methods

Landslide detection was adopted a CNNs based on the U-Net. U-Net was proposed to reduce the loss of feature maps and spatial location information of the fully convolutional networks (Ronneverger, 2015). This model and processing steps were based on the previous study (Konishi, 2021). Figure 4 shows the architecture of U-Net. U-Net consists of a contracting path (left side of Figure 4) that convolves input images and extracts features, and an expansive path (right side of Figure 4) that outputs classified images based on the extracted features. In addition, skip connection with the corresponding feature map from the contracting path to the expansive path at corresponding positions. The contracting path consists of repeated convolutions of $3 \times 3$ with a rectified linear unit (ReLU) and max-pooling $2 \times 2$ for down-sampling. The expansive path consists of repeated transposed convolutions of $2 \times 2$ for up-sampling with the ReLU. In addition, concatenations with the corresponding feature map from the contracting path to the expansive path. $256 \times 256$ square images with three or four layers were used for input. 80% of the dataset for training and 20% of the dataset for validation were randomly selected. We prepared 583 small patches as test data that were not used for training. The epoch is set to 100 and the batch size is set to 40. We trained the U-Net for stochastic gradient descent iterations using Adam optimizer with a learning rate of 0.001. The training, validation, and test procedures were performed on a 3.5 GHz Intel Core i7 processor with 128 GB of RAM. The computations were performed using GPGPU (General Purpose Graphics Processing Units) using an NVIDIA GeForce RTX 3090 graphics card with 24 GB of RAM.

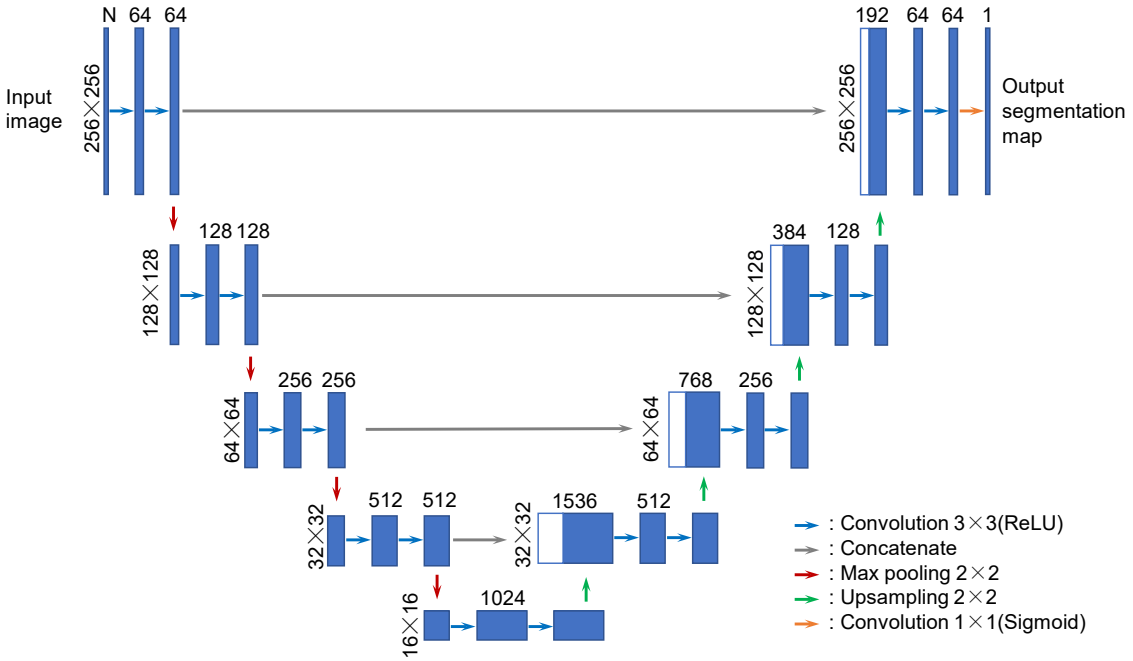


Figure 4. The architecture of U-Net.

### 2.4 Validation Process

To validate the performance of the models, we selected the F1-score based on recall and precision. The precision indicates the percentage of positive results that are correct in the true case. The recall indicates the percentage of positive results that are correct in the actual case. The F1-score is the harmonic mean of the model's precision and recall. The definitions are as follows,

$$\text{Precision} = \frac{TP}{FP + TP}, \tag{1}$$

$$\text{Recall} = \frac{TP}{FN + TP}, \tag{2}$$

$$\text{F1} - \text{score} = \frac{2 \cdot \text{Precision} \cdot \text{Recall}}{\text{Precision} + \text{Recall}}, \tag{3}$$

where true positive (*TP*) is the number of correct detection pixels, False positive (*FP*) is the number of incorrect detection pixels, false negative (*FN*) is the number of landslide pixels note extracted.

## 3. RESULTS AND DISCUSSION

We performed landslide detection using U-Net from SPOT-7 four datasets, which are (1) blue, green, red and NIR, (2) blue, green and red (3) green, red and NIR, (4) blue, green and NDVI. The landslide detection results were validated by the F1-score. Table 1 shows the results of landslide detection for each dataset in the test data. As the result, the highest value of the F1-score in the test accuracy was obtained at 0.828 with the dataset (4). NDVI is more effective than original bands (red and NIR) for landslide detection. Figure 6 shows an example image of landslide detection in the test data. The extent of landslide areas detected by U-Net is smoother than the validation map as shown in Figure 5(a). Dataset (4), shown in Figure 6 (d), which obtained the highest value, has superior detection of the landslide area at the top region of the image. This area was affected by shadows as seen in Figure 5 (b), and the dataset performed well in extracting this area.

Table 1. Results of landslide detection for each dataset in the test data.

| Dataset | Precision | Recall | F1-score |
|---|---|---|---|
| (1) blue, green, red and NIR | 0.764 | 0.891 | 0.823 |
| (2) blue, green and red | 0.693 | 0.889 | 0.779 |
| (3) green, red and NIR | 0.708 | 0.899 | 0.792 |
| (4) blue, green and NDVI | 0.794 | 0.866 | 0.828 |

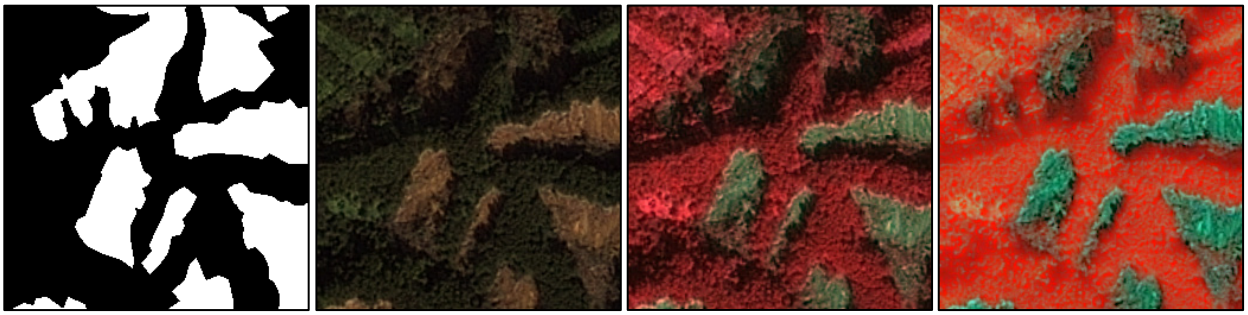

(a) (b) (c) (d)

Figure 5. Comparison of validation map and different band combination of SPOT-7. (a) validation map, (b) R: red, G: green, B: blue, (c) R: NIR, G: red, B: green, (d) R: NDVI, G: green, B: blue.

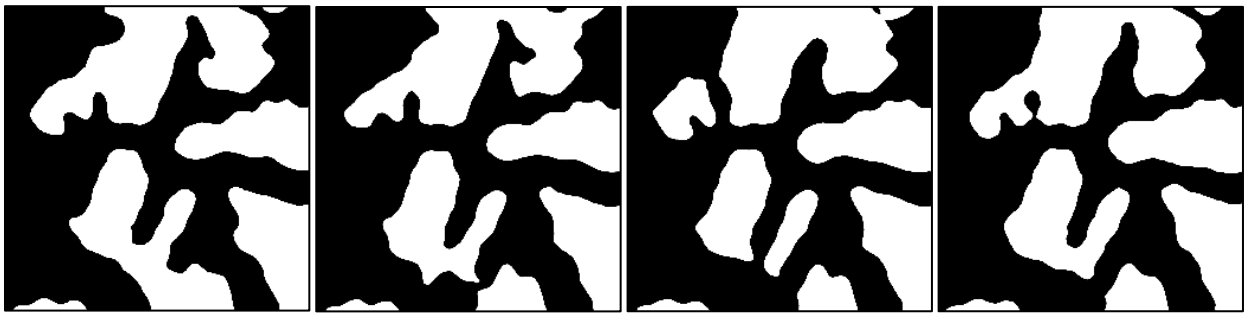

(a) (b) (c) (d)

Figure 6. Comparison of results on the example image patch using different datasets. (a) dataset (1), (b) dataset (2), (c) dataset (3), (d) dataset (4).

## 4. CONCLUSION

In this study, landslide detection using U-Net was performed on four different SPOT-7 band combination datasets. Using GSI's slope failure and sediment distribution map from the case of the 2018 Hokkaido Eastern Iburi Earthquake, we have verified the optimal combination of bands in the SPOT-7 as input data. The highest value of the F1-score in the test accuracy was obtained at 0.828 with the dataset (4) blue, green and NDVI. This result suggests that NDVI is more effective than the original bands (red and NIR) as input for landslide detection.


## ACKNOWLEDGMENTS

This work was supported by JSPS KAKENHI Grant Number JP20K05054.


## REFERENCES


Bragagnolo, L., Rezende, L. R., Silva, R. V. da, Grzybowski, J. M. V., 2021. Convolutional neural networks applied to semantic segmentation of landslide scars, Catena, Vol. 201, 105189.

Fire and Disaster Management Agency (FDMA), 2019. Damage caused by the 2018 Hokkaido Eastern Iburi earthquake and activities of fire and disaster management organizations (Part 34), Retrieved August 18, 2022, from https://www.fdma.go.jp/disaster/info/items/saigaizyohou_07.pdf (in Japanese).

Geospatial Information Authority of Japan (GSI), 2018. Information of 2018 Hokkaido Eastern Iburi earthquake, Retrieved August 18, 2022, from http://www.gsi.go.jp/BOUSAI/H30-hokkaidoiburi-east-earthquake-index.html (in Japanese).

Hexagon, 2022. ERDAS IMAGINE HELP, HPF Resolution Merge.

Japan Meteorological Agency (JMA), 2018. The 2018 Hokkaido Eastern Iburi earthquake sequence (Part 9),

Retrieved August 18, 2022, from https://www.jma.go.jp/jma/press/1809/20a/kaisetsu201809201500.pdf (in Japanese).
Konishi, T., Ito, S., and Oguro, Y., 2021. Landslide extraction with COSMO-SkyMed imageries using U-Net, Proc. SPIE 11861, Microwave Remote Sensing: Data Processing and Applications, 118610H.
Long, J., Shelhamer, E., and Darrell, T., 2015. Fully Convolutional Networks for Semantic Segmentation, IEEE Conference on Computer Vision and Pattern Recognition, pp. 1-12.
Ronneberger, O., Fischer, P., and Brox, T., 2015. U-net: Convolutional networks for biomedical image segmentation, pp. 1-8.
Soares, L. P., Dias, H. C., & Grohmann, C. H., 2020. Landslide Segmentation with U-Net: Evaluating Different Sampling Methods and Patch Sizes, arXiv:2007.06672.
Tofani, V., Hong, Y., and Singhroy, V., 2014. Introduction: Remote Sensing Techniques for Landslide Mapping and Monitoring, Landslide Science for a Safer Geoenvironment, Vol. 2, pp. 301-303.
Zhong, C., Liu, Y., Gao, P., Chen, W., Li, H., Hou, Y., Nuremanguli, T., and Ma, H., 2020. Landslide mapping with remote sensing: challenges and opportunities, International Journal of Remote Sensing, 41(4), pp. 1555-1581.